Linear Contributions of Different Time Scales to Teleconnectivity

PANOS J. ATHANASIADIS

Department of Atmospheric Sciences, University of Washington, Seattle, Washington

MAARTEN H. P. AMBAUM

Department of Meteorology, University of Reading, Reading, United Kingdom

(Manuscript received 7 July 2008, in final form 15 December 2008)

ABSTRACT

The contributions of different time scales to extratropical teleconnections are examined. By applying empirical orthogonal functions and correlation analyses to reanalysis data, it is shown that eddies with periods shorter than 10 days have no linear contribution to teleconnectivity. Instead, synoptic variability follows wavelike patterns along the storm tracks, interpreted as propagating baroclinic disturbances. In agreement with preceding studies, it is found that teleconnections such as the North Atlantic Oscillation (NAO) and the Pacific–North America (PNA) pattern occur only at low frequencies, typically for periods more than 20 days. Low-frequency potential vorticity variability is shown to follow patterns analogous to known teleconnections but with shapes that differ considerably from them. It is concluded that the role, if any, of synoptic eddies in determining and forcing teleconnections needs to be sought in nonlinear interactions with the slower transients. The present results demonstrate that daily variability of teleconnection indices cannot be interpreted in terms of the teleconnection patterns, only the slow part of the variability.

1. Introduction

Early studies of teleconnections used monthly means of meteorological variables, such as surface pressure, to define teleconnection patterns through temporal correlations between noncontiguous areas (e.g., Walker 1923; Wallace and Gutzler 1981). Blackmon et al. (1984a,b) showed that teleconnectivity is a low-frequency phenomenon, since in their study correlation patterns for synoptic and intermediate-frequency transients were found to be associated with mobile anomalies unlike teleconnections, which are large-scale patterns characterized by spatial stationarity. Here, we further amplify and extend these results by presenting new diagnostics demonstrating the contributions (or lack thereof) of different time scales to teleconnectivity.

We consider whether the synoptic transients are part of the variability related to the teleconnections. In the present study, variability from synoptic to intraseasonal time scales is partitioned into distinct frequency bands, and the contribution of each frequency band to dominant extratropical telecorrelations is examined. Empirical orthogonal function (EOF) analysis is also applied to the component time series, and the results are compared with the correlation analysis. In agreement with the findings of Blackmon et al. (1984a,b), our study shows that synoptic transients do not contribute to teleconnections, as they exhibit very different patterns of variability associated with propagating disturbances along the storm tracks. This result brings into question the meaning of daily teleconnection indices [in use, e.g., by the National Oceanic and Atmospheric Administration (NOAA), available online at http://www.cpc.noaa.gov], since high-frequency anomalies obviously affect the values of such indices, which therefore do not meaningfully represent the phase of the underlying teleconnection occurring at lower frequencies. It is suggested that when daily data are used in producing indices for climate variability patterns, high-frequency transients should be filtered out.

Another important point concerns the role of synoptic eddies for driving and determining those teleconnections. The results of this study make it clear that

Corresponding author address: Dr. Panos J. Athanasiadis, Department of Atmospheric Sciences, University of Washington, Box 351640, Seattle, WA 98195-1640.
E-mail: panos@atmos.washington.edu

DOI: 10.1175/2009JCLI2707.1

if synoptic eddies play a role in the dynamics of teleconnections, this has to be through nonlinear processes involving interactions between transients of different time scales. Various recent studies explore such nonlinear interactions, such as the wave breaking mechanism proposed by Benedict et al. (2004). Our study shows that linear mechanisms for synoptic contributions to teleconnections, implicit in Gerber and Vallis (2005), seem to be inconsistent with the reanalysis data.

This article is structured as follows: The dataset used and some computational details that are part of the data processing are described in section 2. Results of the correlation decomposition analysis for the North Atlantic Oscillation (NAO) and the Pacific–North America (PNA) teleconnections are shown in section 3 and corresponding results from the related EOF analysis of the component time series are presented in section 4. Section 5 is a summary of the main conclusions.

2. Data and processing

Daily means for geopotential height at 500 hPa (Z500), mean sea level pressure (MSLP), and potential vorticity at 350 K (PV350) are used from the 40-yr European Centre for Medium-Range Weather Forecasts Re-Analysis (ERA-40) dataset (Uppala et al. 2005). The subsets cover the Northern Hemisphere on a Gaussian grid (N40) with a spatial resolution of approximately 2.25° × 2.25°. For comparison, the analysis for MSLP and Z500 has been repeated using corresponding data with a comparable resolution from the National Center for Atmospheric Research and National Centers for Environmental Prediction (NCEP–NCAR) reanalysis (Kalnay et al. 1996). As Northern Hemisphere teleconnections appear stronger and more consistent in winter (Barnston and Livezey 1987), the period December–March (DJFM) has been chosen for this study. The time series used consist of 45 DJFM seasons (1956–2002), hereafter also referred to as winters, each 121 days long.

The seasonal cycle has a regular and well-defined signature that needs to be removed before we can examine the remaining patterns of variability. For this, the daily climatology has been subtracted from the time series. The daily climatology is calculated by taking the average of the daily means over the years at each grid point. The statistical day-to-day variations have been smoothed out by fitting a fourth order polynomial to the DJFM daily climatology at each grid point. We tested other smoothing methods, such as running means, and found only minimal differences in our results.

Using Fourier filtering, the daily time series are decomposed into orthogonal components (the components are mutually uncorrelated), corresponding to the following frequency bands:

band 1: (2–10 days)
band 2: (10–20 days)
band 3: (20–60 days)
band 4: (60–120 days)

The cutoff frequencies have been chosen so as to split the total variance into approximately equal parts. In particular, we chose this to be true for MSLP at Iceland, but it also holds for most grid points in the extratropics. At each grid point, a fast Fourier transform (FFT) is applied to each individual wintertime series and after setting the coefficients of the components that lie outside a frequency band to zero; applying the inverse transform gives the component time series for this particular band. Because of the discrete nature of the Fourier frequency spectrum, the actual cutoff frequencies are an approximation to the ones shown earlier. No tapering has been used for the Fourier transforms, since regarding the 121-day time series as periodic does not induce any jumps larger or steeper than the often big day–to–day pressure variations. Therefore, this approach does not create unreasonable fictitious components more than the tapering itself would do.

3. Correlation analysis

One-point correlation maps for daily and monthly means are compared. For a particular center of action (Wallace and Gutzler 1981), such a map shows Pearson's linear correlation coefficient calculated at every point as

$$r = \frac{\mathrm{Cov}(X, Y)}{\sqrt{\mathrm{Var}(X)\,\mathrm{Var}(Y)}}, \tag{1}$$

where X and Y are time series of contemporaneous observations, $[(x_i, y_i); i = 1, 2, \ldots N]$, where we fix one of the data points, say, X, at the center of action and then compute the correlation over all Y. Covariance and variance, with the usual definitions, are denoted as Cov and Var.

Figures 1 and 2 show the corresponding correlation maps for the NAO (Icelandic) and the PNA (North Pacific) centers of action. The Icelandic and North Pacific centers are taken approximately at 65°N, 22°W and 45°N, 167°W, respectively. Notice that the correlation patterns for the daily data are less pronounced than the ones calculated from the monthly means. As shown with the following analysis, this is because high frequencies contain a lot of uncorrelated variance, which adds to the denominator in Eq. (1) but leaves the covariance in the

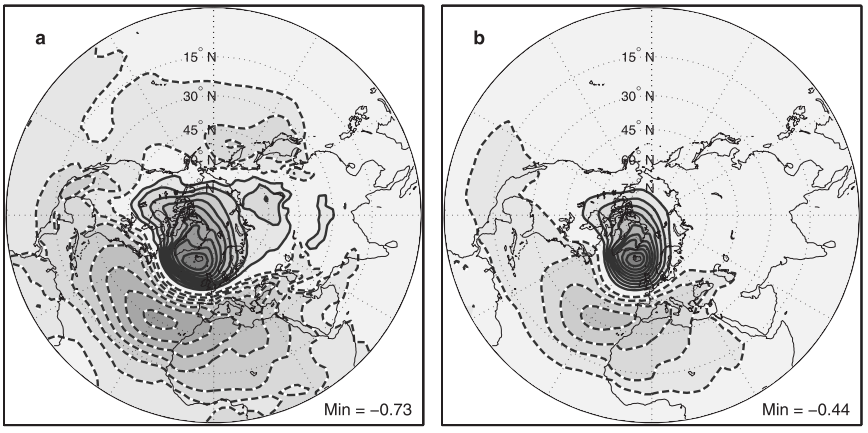

FIG. 1. Teleconnection maps for Iceland, MSLP in DJFM from ERA-40 for (a) monthly and (b) daily means. Contours are every 0.1, with dashed for negatives and the zero contour omitted. The anticorrelation maximum is quoted at the bottom-right corner of each plot (as Min).

numerator largely unchanged at the points concerned. For the NAO, the anticorrelation center at Azores shows a maximum of −0.71 for monthly means but only −0.43 for daily means. For the same reason as given earlier, the secondary anticorrelation center at the North Pacific is lost in the daily means correlation map (Fig. 1b). Similarly, for the PNA the anticorrelation maxima over the North Pacific are −0.61 and −0.79 for daily and monthly means, respectively; here and later Z500 is used for PNA, since this teleconnection has a weak signature at the surface.

To quantify the contribution to these teleconnection patterns by transients at different frequency bands, we employ a new diagnostic. Using Fourier filtering, as described in the previous section, the time series are partitioned in the frequency domain. Then, given the orthogonality of Fourier components, the total covariance can be expressed as the sum of the covariances of the component time series plus a contribution due to winter-to-winter variability (DJFM means), hereafter referred to as the leftover component or "band 0." The contribution of each frequency band to the daily teleconnection pattern is assessed by plotting the following quantity:

$$r_j = \frac{\mathrm{Cov}(X_j, Y_j)}{\sqrt{\mathrm{Var}(X)\,\mathrm{Var}(Y)}}, \tag{2}$$

for $j = 1, 2, 3, 4$: X_j and Y_j represent the corresponding band-filtered time series components; and making the notation compact, for $j = 0$: X_0, and Y_0 are the time series of the winter means that make up the leftover component. Covariance is additive over the bands and therefore

$$r = \sum_{j=0}^{4} r_j. \tag{3}$$

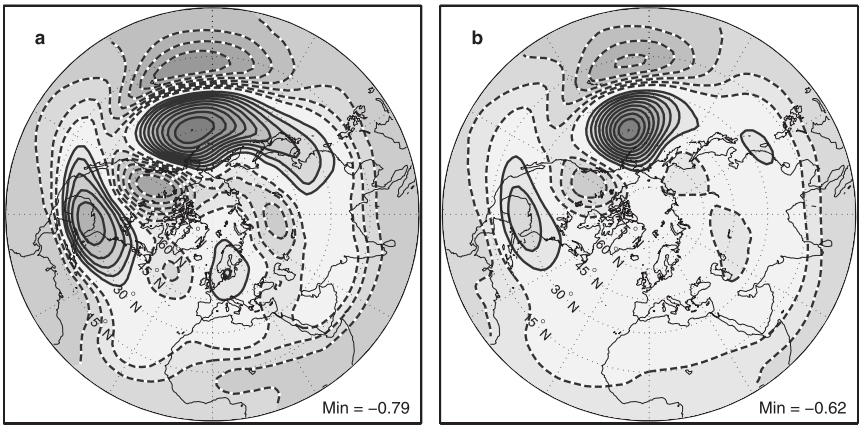

FIG. 2. As in Fig. 1, but for the North Pacific center and for geopotential height at 500 hPa.

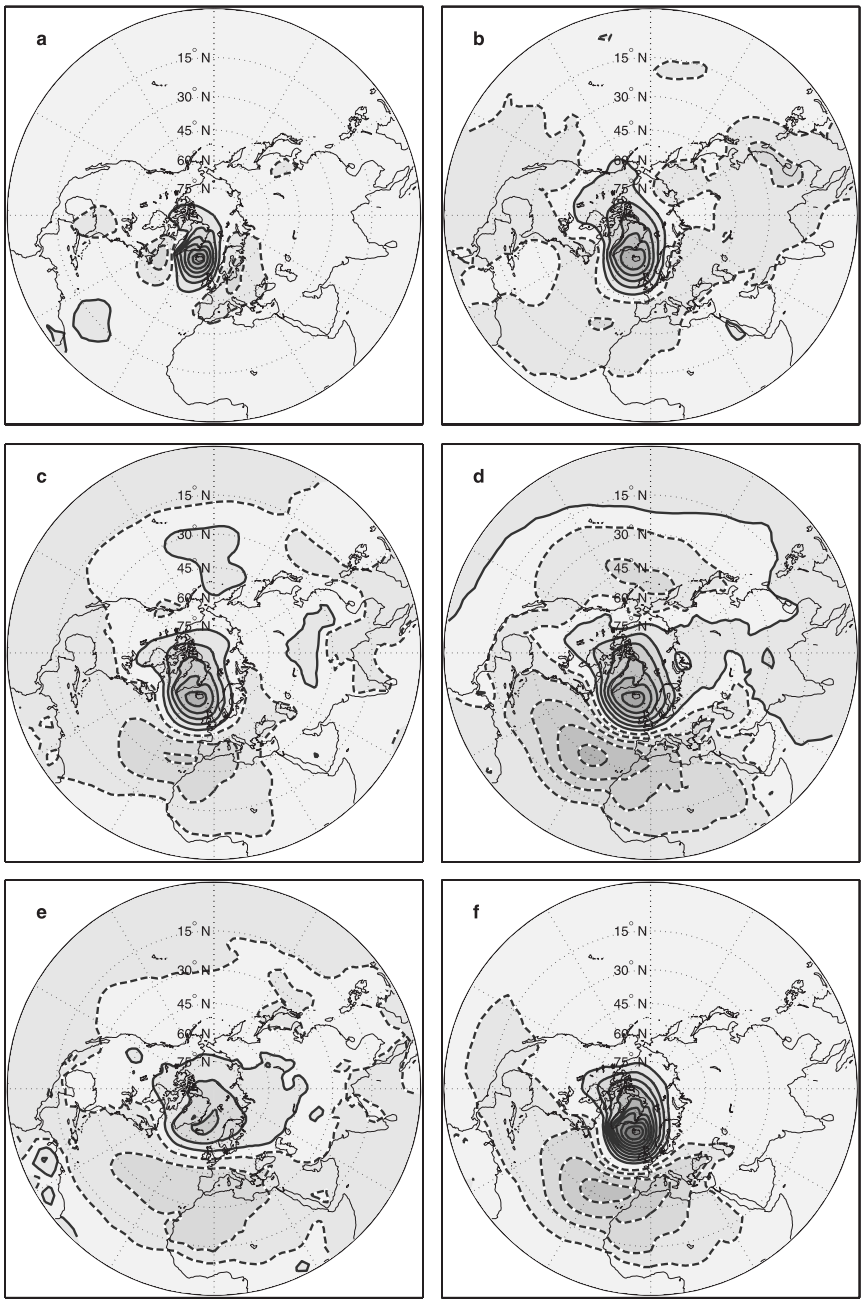

FIG. 3. Contributions to the daily MSLP correlation map for Iceland for (a)–(d) bands 1–4 and (e) band 0. Contour interval is 0.04, with dashed for negatives. (f) Sum of (a)–(e) with contours as in Fig. 1, allowing for comparison with the respective daily correlation map.

This correlation decomposition method is first applied to the NAO daily teleconnection pattern using MSLP for the bands described previously. Figure 3 shows the contribution of each band for the case of the Icelandic center. Adding the corresponding five fields, we recover the teleconnection pattern for daily means [Eq. (3)] within the computational accuracy of the fast Fourier transform routine and its inverse and the cumulative rounding errors. As mentioned previously, the cutoff frequencies that define the four frequency bands have been chosen so as to partition the total variance into approximately equal parts. Therefore, the contributions to the daily correlation by these bands, as shown in the figure, can be justly compared to each other.

Band 4 exhibits a pattern very similar to the monthly correlation map. It is characterized by a strong dipole pattern over the North Atlantic, and it also has a secondary anticorrelation center in the North Pacific. This is reasonable, since here the high-frequency uncorrelated variance is filtered out. Band 4 predominantly determines the NAO teleconnection, as one can see comparing the contributions of the different bands. Band 3 also contributes to the NAO dipole, but the anticorrelation with the North Pacific is almost lost.

Band 1 is totally different, and it does not contribute at all to the NAO pattern. Instead, it exhibits a wave train pattern with a zonal orientation. This behavior is understood by considering the wavy character of the anomalies associated with synoptic systems traveling along the North Atlantic storm track. This argument is in agreement with the results of Blackmon et al. (1984b), who find that these zonally oriented, smaller-scale, wavelike features are mobile, and they propagate with a speed comparable to the ambient wind at 700 hPa. In contrast, teleconnections are larger-scale stationary patterns. Band 2 exhibits an intermediate behavior, sharing some similarity with band 1 and band 3 and having a small contribution to the Azores' anticorrelation. The latter is also the case for the leftover component.

This analysis was repeated using NCEP–NCAR reanalysis data for the same years and gave essentially the same results. Also, the analysis was applied to other centers of action in the Euro-Atlantic sector (not shown) as well as to the PNA center in the North Pacific (Fig. 4) for Z500. As far as the character of each band contribution is concerned, the results are broadly similar to the NAO case. The common conclusions that can be drawn are as follows:

- Teleconnections occur in low-frequency variability (band 4, band 3, and band 0).
- Variability at intermediate time scales (band 2) does not show a distinct behavior.
- Synoptic variability (band 1) does not have a linear contribution to teleconnectivity.

4. EOF analysis

To examine the behavior of variability at the different frequency bands, we have also employed EOF analysis. As discussed below, this is a different and somewhat complementary analysis to the teleconnections approach. Computing EOFs for bandpassed time series of various fields allowed for comparison with the results of the correlation analysis.

Although correlation analysis examines the variability in respect to the primary centers of action of given teleconnections, the EOF analysis is not point centric, and it is also not specifically designed to highlight regional patterns of strong correlation. Instead it gives one by one the leading patterns along which the analyzed dataset exhibits most of its variance. Also, Ambaum et al. (2001) point to the fact that EOFs cannot have a local interpretation, in the sense that the loadings at every two points do not simply depend on the temporal correlation between the time series at these points. Instead, local loadings depend on the whole dataset. This nonlocal nature differentiates EOFs from correlation analysis. Reviewing EOF analysis, Richman (1986) points to a number of other inherent drawbacks, such as the domain–shape dependence (arising from the orthogonality constraint) and the often inaccurate portrayal of existing physical relationships. EOF analysis as a sole statistical tool does not necessarily point to entities with physical meaning, and care is always needed in interpreting the results. In the absence of dominant telecorrelations in the data (patterns with strong temporal coherency), EOF analysis tends to give monopolar structures. All these properties make it nontrivial as to whether EOF analysis would corroborate the results of our correlation analysis.

Using the same Fourier decomposition of the daily time series, EOF analysis is carried out for MSLP, Z500, and PV350 at the same frequency bands. As for the correlation analysis, daily DJFM time series are used, and the seasonal cycle is similarly removed. Note that tropical variability does not seem to influence the calculated EOFs. Therefore, the whole hemispheric domain was retained. Area weighting has been applied to account for the uneven data grid, as shown in North et al. (1982), and the resulting EOFs are scaled so as to carry the units of the data; this way, the norm of each EOF is also proportional to the corresponding "explained variance," which is desirable for comparing individual EOFs (Wilks 1995). A few leading EOFs were examined for each field and frequency band; in this paper, only the first EOFs are presented.

In Fig. 5 the first EOF (EOF 1) is shown for each of the frequency bands and for monthly mean data, all for MSLP. Although the EOF patterns are not expected to be the same as the correlation maps, we note the clear resemblance between the EOFs and the correlation maps for the same bands. The correlation and EOF analyses are consistent, in that they demonstrate the fundamentally different behavior of the variability at different time scales. EOFs for synoptic transients exhibit the same wave train patterns as the correlation analysis has shown. A very similar pattern arises when analyzing the Z500 field. Apparently, baroclinic eddies dominate the variability in band 1 so much as to

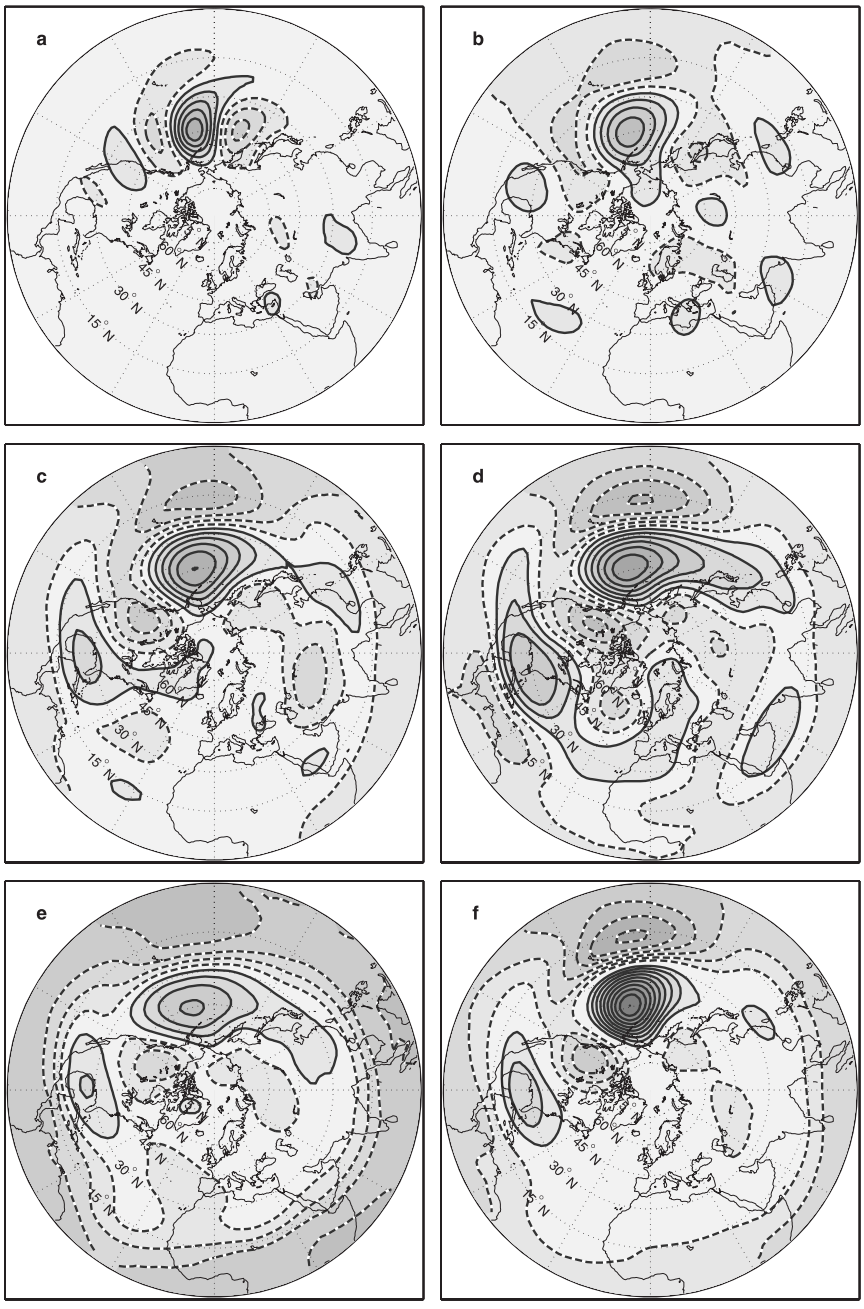

FIG. 4. As in Fig. 3, but for daily Z500 correlation map for North Pacific and with contours as in Fig. 2.

counteract the domain dependence of the first EOF. The results demonstrate the strong temporal and spatial coherence of the synoptic waves. The same is true at higher levels, as seen in Fig. 6, showing the respective EOFs for PV350. In the latter plots, there is a clear distinction between the zonally propagating synoptic waves and the meridionally oriented, low-frequency patterns related to jet stream variability.

The presented EOFs are found to be well separated from the following EOFs and therefore are expected to be relatively unaffected by sampling issues (North et al. 1982). The band-1 EOFs, representing wave trains, all come in pairs that are in quadrature (not shown). These paired EOFs are well separated from the following in-rank EOFs; although they are much less separated from each other; together they represent a single traveling wave.

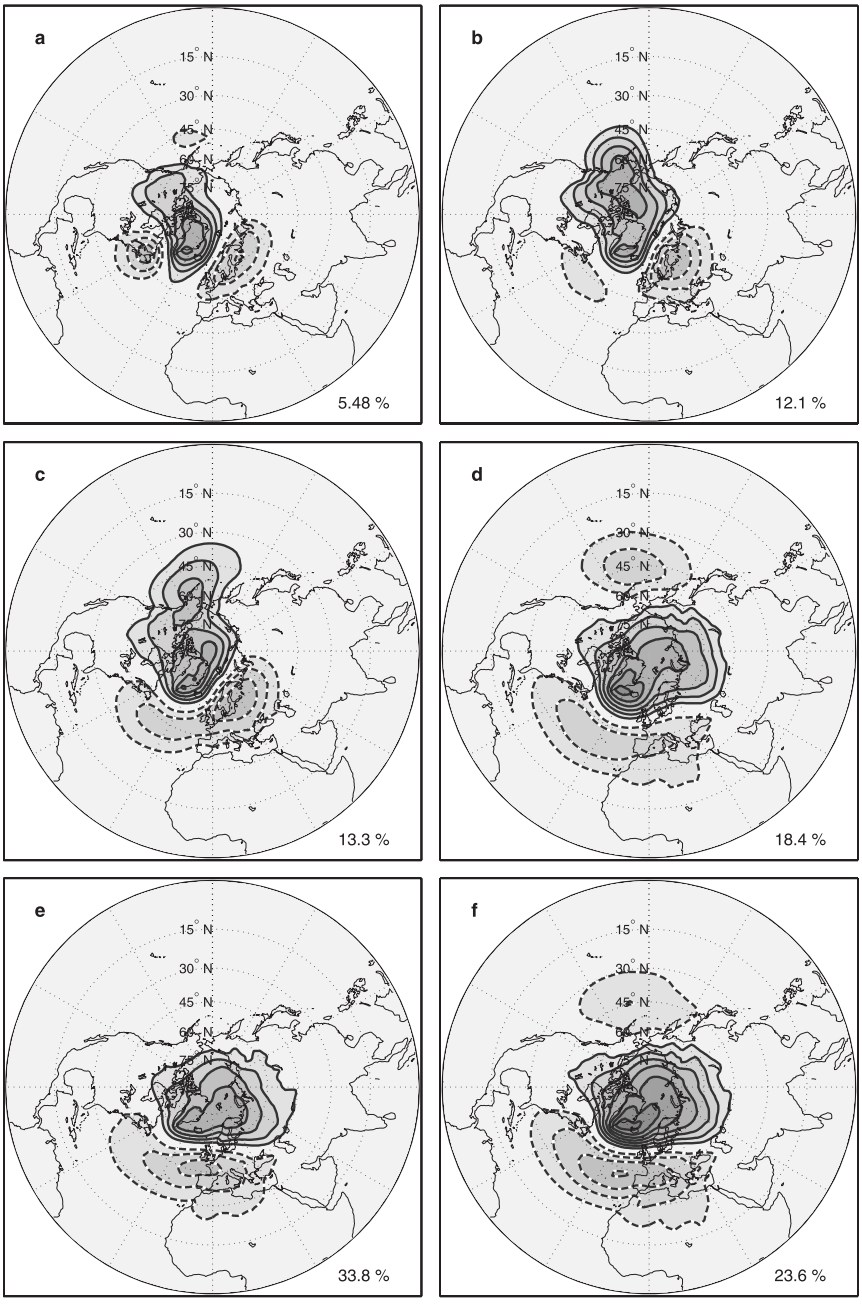

FIG. 5. MSLP EOF 1 for DJFM for (a)–(d) frequency bands 1–4, (e) band 0, and (f) monthly means. The contour interval is 0.5 hPa, with the zero contour omitted. Explained variances are quoted as percentages.

The band-1 EOFs represent small amounts of the corresponding total variance (Figs. 5 and 6), although the leading EOFs have a similar character under zonal rotations and make up the majority of the variance in that band. Therefore, it is argued that a set of these weak EOFs jointly represent the same type of synoptic transients behavior as in the North Atlantic or in the North Pacific sectors. Also, as shown by Horel (1981), rotation of a subset of the leading EOFs for monthly Z500 can yield patterns that are more similar to familiar teleconnections than the presented ordinary EOFs (Fig. 6f).

To summarize: the high-frequency variability (band 1) is dominated by wavelike patterns of variability consistent with propagating baroclinic disturbances, while progressively, from band 2 to band 4 and to interannual variability, the patterns transform into the known climate

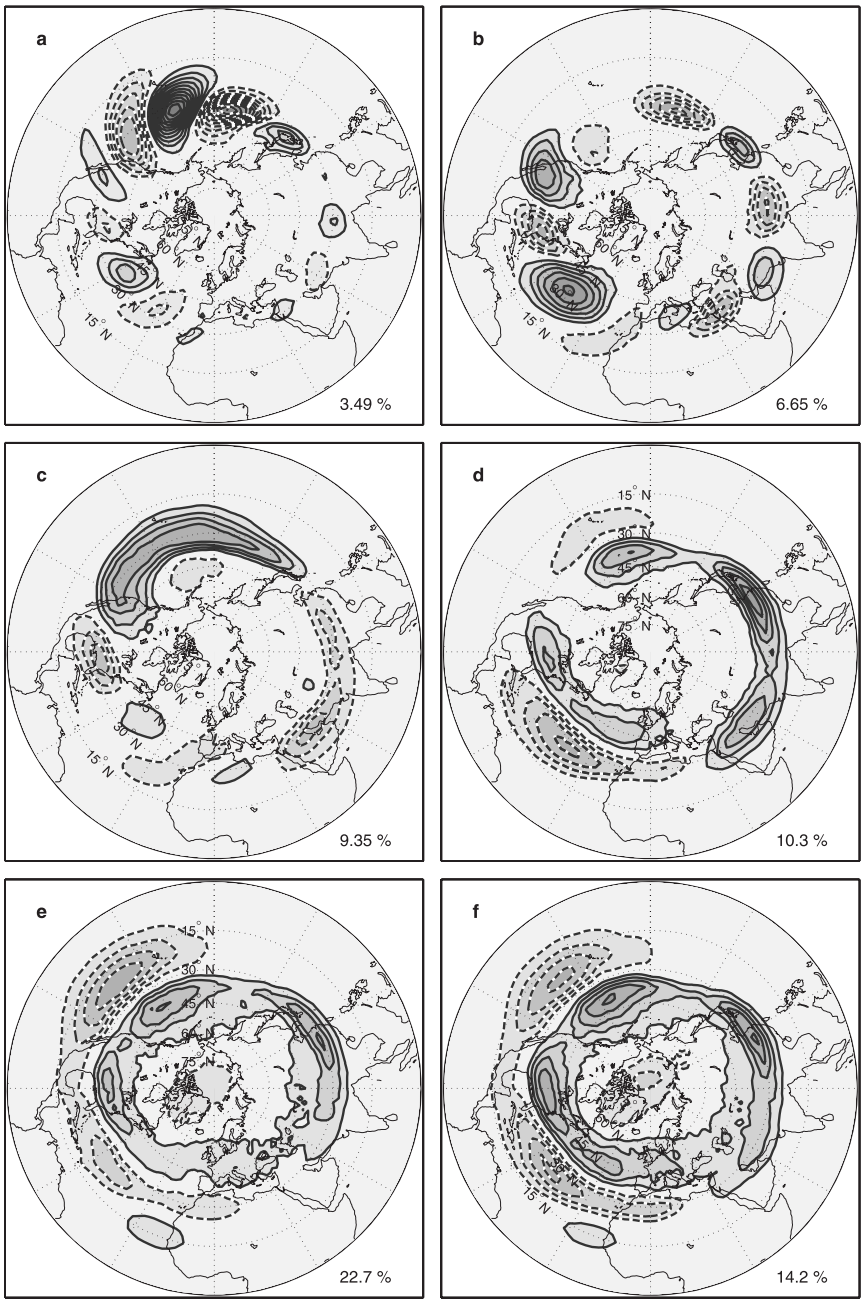

FIG. 6. As in Fig. 5, but for PV350 EOF 1; the contour interval is 0.1 PVU, with the zero contour omitted.

variability patterns, starting with the NAO dipole (for MSLP).

5. Summary

We have examined the role of transient eddies of different time scales (synoptic to intraseasonal) for contributing to teleconnectivity associated with the leading patterns of variability in the extratropics, such as the NAO and the PNA. These teleconnections are well documented and are usually defined using monthly means of geopotential or sea surface pressure. They are stationary large-scale correlation patterns.

Our analysis, based on decomposing daily data time series into components for a number of frequency bands, shows that synoptic variability (2–10 days) does

not contribute to the temporal correlations constituting the examined teleconnections. Hence, synoptic-scale transients do not have a linear contribution to these teleconnections. This is in accordance with the findings of Blackmon et al. (1984b), which show one-point correlation maps for synoptic band-filtered transients to be totally different from teleconnections. Synoptic variability follows patterns that resemble wave trains oriented along the storm tracks and are interpreted as propagating baroclinic disturbances. Variability at intermediate time scales (10–20 days) has a mixed character, and as shown by Blackmon et al. (1984b), the associated patterns (in contrast to teleconnections) relate to mobile anomalies.

Teleconnections were found to occur only in low-frequency variability (20 days and beyond). This does not exclude the faster synoptic transients for playing a role in teleconnections dynamics, yet our results suggest that a nonlinear (cross band) interaction is required for this role. A number of studies, such as Vallis et al. (2004) and Lorenz and Hartmann (2003), examine the role of nonlinear interactions between synoptic and slower anomalies using modeling and diagnostic approaches. Wave breaking, as suggested by Benedict et al. (2004), is a possible mechanism for such an interaction. On the other hand, in view of our results, the mathematical model of Gerber and Vallis (2005) probably presents only a partial picture, in that the NAO-like dipole patterns they produce do not depend on the temporal structure of the signal, whereas we find that the temporal structure is important, because the synoptic eddies satisfy the same constraints as in the Gerber and Vallis random walk model, but the reanalysis data show that the synoptic variability does not exhibit meridional dipoles. In other words, momentum or mass conservation under given meridional boundary conditions is not in itself sufficient for explaining the meridional dipole patterns seen in extratropical low-frequency variability, since these quantities are conserved at all time scales, whereas no such dipoles are found in synoptic variability.

From the presented analysis, it also follows that teleconnection indices exhibiting high-frequency variability do not reliably portray the phase of the corresponding teleconnection because the value of such indices is strongly affected by the synoptic anomalies, which do not exhibit teleconnectivity. In other words, we can use a daily index calculated without low-pass filtering but we cannot say, for example, that the NAO is in its positive phase when this index is positive. To make this better understood, consider the case where all anomalies—not only the synoptic ones—at the centers of action of a particular teleconnection occurred unpaired; we could still define the same varying teleconnection index, although a teleconnection would not actually exist (no correlation). Daily variability of teleconnection indices cannot be interpreted in terms of the teleconnection patterns, only the slow part of the variability.

Acknowledgments. The authors are grateful to the Joint Institute for the Study of the Atmosphere and Ocean (JISAO) for covering the publishing charges.

REFERENCES

Ambaum, M. H. P., B. Hoskins, and D. Stephenson, 2001: Arctic Oscillation or North Atlantic Oscillation? *J. Climate,* **14,** 3495–3507.

Barnston, A. G., and R. Livezey, 1987: Classification, seasonality and persistence of low-frequency atmospheric circulation patterns. *Mon. Wea. Rev.,* **115,** 1083–1126.

Benedict, J. J., S. Lee, and S. Feldstein, 2004: Synoptic view of the North Atlantic Oscillation. *J. Atmos. Sci.,* **61,** 121–144.

Blackmon, M. L., Y.-H. Lee, and J. Wallace, 1984a: Horizontal structure of 500 mb height fluctuations with long, intermediate and short time scales. *J. Atmos. Sci.,* **41,** 961–979.

——, ——, ——, and H.-H. Hsu, 1984b: Time variation of 500 mb height fluctuations with long, intermediate and short time scales as deduced from lag-correlation statistics. *J. Atmos. Sci.,* **41,** 981–991.

Gerber, E. P., and G. Vallis, 2005: A stochastic model for the spatial structure of annular patterns of variability and the North Atlantic Oscillation. *J. Climate,* **18,** 2102–2118.

Horel, J. D., 1981: A rotated principal component analysis of the interannual variability of the Northern Hemisphere 500 mb height field. *Mon. Wea. Rev.,* **109,** 2080–2092.

Kalnay, E., and Coauthors, 1996: The NCEP/NCAR 40-Year Reanalysis Project. *Bull. Amer. Meteor. Soc.,* **77,** 437–472.

Lorenz, D. J., and D. Hartmann, 2003: Eddy-zonal flow feedback in the Northern Hemisphere winter. *J. Climate,* **16,** 1212–1227.

North, G. R., T. Bell, and R. Cahalan, 1982: Sampling errors in the estimation of empirical orthogonal functions. *Mon. Wea. Rev.,* **110,** 699–706.

Richman, M. B., 1986: Rotation of principal components. *J. Climatol.,* **6,** 293–335.

Uppala, S. M., and Coauthors, 2005: The ERA-40 re-analysis. *Quart. J. Roy. Meteor. Soc.,* **131,** 2961–3012.

Vallis, G. K., E. Gerber, P. Kushner, and B. Cash, 2004: A mechanism and simple dynamical model of the North Atlantic Oscillation and annular modes. *J. Atmos. Sci.,* **61,** 264–280.

Walker, G. T., 1923: Correlation in seasonal variation of weather, VIII: A preliminary study of world weather. *Mem. Indian Meteor. Dept.,* **24,** 75–131.

Wallace, J. M., and D. Gutzler, 1981: Teleconnections in the geopotential height field during the Northern Hemisphere winter. *Mon. Wea. Rev.,* **109,** 784–812.

Wilks, D. S., 1995: *Statistical Methods in the Atmospheric Sciences: An Introduction*. International Geophysics Series, Vol. 59, Academic Press, 467 pp.